Studies on the Adsorption and Desorption of Mitoxantrone to Lauric Acid/Albumin Coated Iron Oxide Nanoparticles

Jan Zaloga[1,†], Artem Feoktystov[2,†], Vasil M. Garamus[3,†], Weronika Karawacka[1], Alexander Ioffe[2], Thomas Brückel[4], Rainer Tietze[1], Christoph Alexiou[1,*] and Stefan Lyer[1]

1 Department of Otorhinolaryngology, Head and Neck Surgery, Section for Experimental Oncology and Nanomedicine (SEON), Else Kröner-Fresenius-Stiftung-Professorship, University Hospital Erlangen, Germany; E-Mail: zaloga@gmx.de (J.Z.); weronika.karawacka@uk-erlangen.de (W.K.); rainer.tietze@uk-erlangen.de (R.T.); c.alexiou@web.de (C.A.); stefan.lyer@uk-erlangen.de (S.L.)

2 Jülich Centre for Neutron Science (JCNS) at Heinz Maier-Leibnitz Zentrum (MLZ), Forschungszentrum Jülich GmbH, Lichtenbergstr. 1, 85748 Garching, Germany; E-Mail: a.feoktystov@fz-juelich.de (A.F.); a.ioffe@fz-juelich.de (A.I.)

3 Helmholtz-Zentrum Geesthacht: Zentrum für Material- und Küstenforschung GmbH, Geesthacht, Germany; E-Mail: vasyl.haramus@hzg.de (V.G.).

4 Jülich Centre for Neutron Science (JCNS-2) and Peter Grünberg Institute (PGI-4), JARA-FIT, Forschungszentrum Jülich GmbH, 52425 Jülich, Germany; E-Mail: t.brueckel@fz-juelich.de (T.B.)

† These authors contributed equally to this work.

* Author to whom correspondence should be addressed; E-Mail: c.alexiou@web.de; Tel.: +49-9131-8534769; Fax: +49-9131-8534828.

Statistical summary (excluding supplementary)

Pages – 26

Words –8341

Number of Figures and Tables – 8 excl. Supplementary

Received: / Accepted: / Published:

Abstract:

A rational use of superparamagnetic iron oxide nanoparticles (SPIONs) in drug delivery, diagnostics, and other biomedical applications requires deep understanding of the molecular drug adsorption/desorption mechanisms for proper design of new pharmaceutical formulations. The adsorption and desorption of the cytostatic Mitoxantrone (MTO) to lauric acid-albumin hybrid coated particles SPIONs ($SEON^{LA\text{-}HSA}$) was studied by Fourier transform infrared spectroscopy (FTIR), dynamic light scattering (DLS), surface titration, release experiments and small-angle neutron and X-ray scattering. Such MTO-loaded nanoparticles have shown very promising results in *in vivo* animal

models before, while the exact binding mechanism of the drug was unknown. SEON^{LA-HSA} formulations have shown better stability under drug loading in comparison with uncoated nanoparticle and sustainable drug release to compare with protein solution. Adsorption of MTO to SEON^{LA-HSA} leads to decreasing of absolute value of zeta potential and repulsive interaction among particles, which points to the location of separate molecules of MTO on the outer surface of LA-HSA shell.

Keywords: magnetic drug targeting; iron oxide nanoparticles; nanomedicine; small-angle scattering of neutrons and X-rays

---

1. Introduction

Superparamagnetic iron oxide nanoparticles (SPIONs) are a very promising vehicle for drug delivery, imaging and several other biomedical applications[1-5]. In Magnetic Drug Targeting (MDT), particles are accumulated in a certain body region using magnetic field gradients[6]. Aggregation behaviour of SPIONs is crucial for proper application and is mostly determined by interface properties. The different approaches of interface modification are used to get particles of proper size in determined medium i.e., the most promising approaches for water based solutions are electrostatic[7] or steric[8] approaches. Furthermore, these coating molecules are also used as binding moieties for pharmacologically active substances. Drugs can thus be concentrated accordingly if they are bound to the SPIONs with sufficient stability. We have demonstrated earlier that the bioavailability of drugs can thus be enhanced over 56-fold, which greatly increases efficacy of therapy and reduces side effects[3]. A pharmaceutically active moiety can be attached to the particles by either covalent binding or adsorption. While both binding strategies offer advantages and disadvantages[9] it is important to understand the binding location of drugs in order to understand the drug release *in vivo* as well as the influence of drug binding on important particle characteristics such as colloidal stability, hydrodynamic size or surface charge. For potential use in complex biosystems, i.e. *in vivo*, it is thus preferable to understand the mechanism of drug binding to the particles and its influence on their ordering and stability[10]. Recently we have reported about a hybrid lauric acid/human serum albumin coated formulation called SEON^{LA-HSA}. These particles showed very promising properties for MDT after the cytotoxic drug mitoxantrone (MTO) was added to the particle suspension to yield SEON$^{LA-HSA*MTO}$ [11]. The stabilisation mechanism of SEON^{LA-HSA} seemingly is a mixture between electrostatic and steric stabilisation. While MTO showed a slow, pseudo-zero order release kinetics from SEON$^{LA-HSA*MTO}$ the exact binding location remains unclear. Due to its chemical nature MTO possesses charged, polar groups as well as a conjugated π system. This gives rise to its amphiphilic nature, as the logarithm of its partition coefficient in n-octanol/water (log*P* value) lies at −3.1[12]. MTO shows significant and specific binding to albumin[13] as well as being a strong complexing agent for iron[14]. Classical methods such as nuclear magnetic resonance (NMR) based spectroscopy are not able to investigate the binding mechanism of MTO to the particles due to the magnetic properties of the particles. Fourier transform infrared spectroscopy (FTIR) or fluorescence spectroscopy did not produce

conclusive results. This, together with the proposed binding modality of MTO to $SEON^{LA\text{-}HSA}$, leaves speculation whether the drug is located at the iron oxide core, in the albumin hull around the particles or even just in the surrounding Helmholtz layers around the individual colloid particles.

In the present study we investigated adsorption and desorption of MTO to different compounds including human serum albumin (HSA), uncoated iron oxide particles and lauric acid/HSA coated particles. We investigated adsorption efficiency and also the desorption kinetics of MTO from the respective compounds using high performance liquid chromatography coupled with ultraviolet detection (HPLC-UV). The effect of surface adsorption on colloidal properties of the system was investigated using dynamic light scattering (DLS), surface titration techniques and FTIR. We furthermore studied structure and interactions of particle clusters using small-angle scattering (SAS) methods. Application of X-rays and neutrons as probes gives us the possibility to visualize different parts of clusters (iron and LA/HSA/MTO) and find out the possible location of MTO by comparison of the alternation of structure and interaction among clusters after drug addition. With our findings we show the effects of surface adsorption and desorption of small molecules on the cluster interaction as well as on the colloidal properties of such materials.

2. Experimental Section

2.1 Chemicals and reagents

Iron (II) chloride tetrahydrate ($FeCl_2 \cdot 4H_2O$) EMSURE quality and deuterium oxide (D_2O) were purchased from Merck (Darmstadt, Germany). Iron (III) chloride hexahydrate ($FeCl_3 \cdot 6H_2O$) Ph. Eur. quality, heavy metal-free dialysis tubes (Spectrapor 7, MWCO 8 kDa), ammonium chloride Ph.Eur quality, hydrochloric acid 25%, sodium chloride, sodium hydroxide, sodium hydrogencarbonate, magnesium sulphate, methanol, formic acid, nitric acid 65% and ammonia solution 25% Ph.Eur quality were supplied by Roth (Karlsruhe, Germany). Lauric acid, Bovine serum albumin (BSA), potassium dihydrogenphosphate, D-glucose and acetone were purchased from Sigma-Aldrich (St Louis, MO, USA). Iron reference standards 1 g/L were bought from Bernd Kraft GmbH (Duisburg, Germany). Recombinant human serum albumin without octanoate stabilization (Albix®) was purchased from Novozymes Biopharma (Bagsvaerd, Denmark). Strata Phenyl columns (500 mg/3 ml) were purchased from Phenomenex (Torrance, CA, USA). Mitoxantrone solution 2 mg/ml was bought from Hexal AG (Holzkirchen, Germany). 500 µL ultrafiltration tubes were bought from Sartorius (Goettingen, Germany). Sterile tangential ultrafiltration columns (MWCO 30 and 100 kDa) were purchased from Spectrum Labs (Los Angeles, USA). Polydiallyldimethylammonium chloride (PolyDAADMAC) was purchased from Waco chemicals GmbH (Neuss, Germany). Deuterated MTO (dMTO) was bought from Toronto Research Chemicals (Toronto, Canada).

2.2. Synthesis of $SEON^{LA\text{-}HSA}$ particles and control particles

$SEON^{LA\text{-}HSA}$ particles were produced according to a previously published protocol[11]. Briefly, the SPIONs were synthesized and coated *in situ* with lauric acid. Therefore, iron (II) and iron (III) chloride were dissolved at a molar ratio of 1:2 in ultrapure water and heated to 90 °C in an Argon atmosphere.

Under constant stirring, NH_3 solution 25% was added to precipitate the magnetite particles. After addition of excess lauric acid and 15 min of stirring which lead to formation of a brownish colloid the particles were purified by dialysis (molecular weight cut-off: 8 kDa). The purified particles were coated by dropwise addition to a purified human serum albumin solution 20%. Excess non-adsorbed albumin was quantitatively removed using an established tangential ultrafiltration method, leaving an iron to albumin ratio of about 18% (m/m)[15]. The total iron content was determined using the microwave plasma - atomic emission spectrometry (MP-AES). For that purpose, three different aliquots (50 µl) of the respective ferrofluid were dissolved in 950 µl of hydrochloric acid 25%. The iron content was then determined with an Agilent 4200 MP-AES (Agilent Technologies, Santa Clara, CA) using an iron solution as external standard.

Uncoated ($SEON^0$) particles, lauric acid only-coated particles ($SEON^{LA}$) and lauric acid/bovine serum albumin particles ($SEON^{LA\text{-}BSA}$) were produced using the same protocol as for above-mentioned precursor. Reaction was stopped after precipitation or after lauric acid addition and the samples were purified by dialysis accordingly. For the synthesis of BSA-coated particles BSA solution 20% (m/V) was prepared in ultrapure water. Lauric acid-rich human serum albumin reference was produced by mixing the same human serum albumin solution with a fivefold molar excess of lauric acid, which is the saturation condition for medium-chain fatty acids[16].

2.3 Drug binding studies

Commercially available MTO solution was purified from its salt byproducts using a Phenomenex Strata Phenyl column. The column was conditioned with methanol, 1 ml of MTO solution (2 mg/ml) was eluted and the MTO was washed with at least 10 ml of 1% formic acid solution in water. The MTO was then eluted from the column using 1% formic acid in methanol. The MTO eluate was collected and dried under vacuum, and the MTO was redispersed in ultrapure water. The MTO content of this solution was determined using a previously described HPLC-UV method[17].

The so-prepared salt-free MTO solution was adsorbed to $SEON^0$ and $SEON^{LA\text{-}HSA}$ particles (total iron concentrations 2 mg/ml) and to a solution of lauric acid-rich HSA (11.1 mg/ml). After 5 minutes of equilibration time the particles were either centrifuged for 10 minutes at 14.000 rpm ($SEON^0$) or purified by ultrafiltration (MWCO 30 kDa) ($SEON^{LA\text{-}HSA}$, HSA). Different methods were chosen because the coated particles and HSA are not quantitatively separable from the solvent by centrifugation. The supernatant/filtrate MTO content was determined using HPLC-UV.

2.4 Drug release studies

The dialysis bag model was used to investigate drug release from $SEON^0$, $SEON^{LA\text{-}HSA}$ and HSA. Therefore 3 ml of the sample (with added MTO mass of 300 µg) were put into a dialysis tube (MWCO 8 kDa). Under gentle shaking the samples were incubated at 37 °C in 62.5 ml of release buffer. As release buffer an aqueous solution of 0.114 M sodium chloride, 0.003 M potassium chloride, 0.0025 M calcium chloride, 0.001 M potassium dihydrogen phosphate, 0.0008 M magnesium sulphate, 0.024 M sodium hydrogen carbonate, 0.1% D-glucose was adjusted to pH 7.04 using hydrochloric acid. At defined time points 3 ml of sample were drawn from the surrounding medium. They were eluted via Phenomenex columns as described in Section 2.3 and the resulting solid was redispersed in Methanol.

Additionally, after 48 h a sample aliquot of 20 µl was dissolved in 980 µl of hydrochloric acid and purified accordingly as control. All samples were analyzed for their MTO content via HPLC-UV.

In order to determine the effect of ionic substances with high affinity to iron oxide surface on the MTO binding we performed a phosphate release assay. Phosphate was chosen because it has a very high affinity towards iron oxide surfaces[7]. To 5 mL of corresponding $SEON^{LA\text{-}BSA}$ 500 µg of MTO were added. 200 µL of $SEON^{LA\text{-}BSA*MTO}$ were diluted to 2 mL with Millipore water or the corresponding dilution of NaH_2PO_4 stock solution ($H_2PO_4^-$ concentrations from 0.0 to 3.5 mM, pH adjusted to 7.1 with NaOH) and incubated for 48 h at 4 °C. The particles were then centrifuged for 1 h at 12700 rpm and the supernatant was taken for analysis. The MTO amounts in the supernatants were determined by HPLC-UV.

2.5 DLS and surface titration

$SEON^{LA\text{-}HSA}$ particles were diluted to a total iron concentration of 2 mg/ml. 100 µg/ml of salt-free MTO solution was added and the suspension was allowed to equilibrate for 5 minutes. The same volume of ultrapure water was added to the particles without MTO in order to adjust the particle concentration. 50 µl of the particle suspension with or without MTO were diluted in 2 ml of ultrapure water and the hydrodynamic size of the particles was recorded in triplicates at 25 °C using a Nanophox (Sympatec, Clausthal-Zellerfeld, Germany). The signal was recorded at a scattering angle of 90° in cross-correlation mode. Autocorrelation function was fitted based on an automatic non-negative least squares fit (auto-NNLS). To compare the degree of polydispersity, the relative distribution width of the non-negative least square Gaussian fit (D_{rel}) was calculated from the quantiles of the distribution using equation 1:

$$D_{\mathrm{rel}} = \frac{x_{90} - x_{10}}{x_{50}} \quad (1)$$

The surface of the particles was titrated using a Stabino particle charge titration analyzer (ParticleMetrix, Meerbusch, Germany). 100 µl of above-mentioned suspensions were diluted in 10 ml of ultrapure water and the zeta potential was titrated between pH 3 and 10 using hydrochloric acid 0.025 N or sodium hydroxide solution 0.025 N. In order to determine the surface charges independent of the pH we used polyelectrolyte titration. 100 µl of the suspension were mixed with 10 µl of phosphate buffer pH 7 (25 mM) and diluted in 10 ml of ultrapure water. The negative charges on the particle surface were titrated using 0.0025 N Polydiallyldimethylammoniumchlorid (PolyDADMAC) solution in constant 15 µl steps. All experiments were performed in triplicates. The titration curves were fitted using a linear or polynomic fit in MS Excel.

2.6 FTIR

100 µl of the particle suspensions from Section 2.5 were freeze-dried overnight. Spectra of the solids were then taken with a BRUKER Alpha FTIR spectrometer (Bruker, Billerica, MA, USA) operated in attenuated total reflection (ATR) mode from 4000 cm^{-1} to 400 cm^{-1} using a step size of 0.5 cm^{-1}.

2.7 Small-angle X-ray scattering (SAXS)

The SAXS experiments were performed at the P12 BioSAXS beamline at PETRA III (EMBL/DESY) in Hamburg, Germany. Photon beam of energy 10 keV with flux of 1 x 10^{13} s^{-1} per spot size of 0.2 mm × 0.1 mm (HxV) was applied. The diffraction patterns were collected with a Pilatus 2M detector (Dectris, Switzerland). An automatic sample changer was employed for data collection. The 20 µl of sample was delivered into a glass capillary (20 °C). 20 diffraction patterns were collected for every sample, each with an exposure time of 0.05 s. Buffer was measured before and after every measurement and the average of both was used as background subtracted from the sample curve. To avoid radiation damage by subsequent illuminations curves showing deviations were discarded by the automated data acquisition software[18]. The instrument was calibrated using silver behenate and the observed *q*-range was 0.03 nm^{-1} to 4.8 nm^{-1}.

Deuterated MTO (dMTO) and conventional MTO were used in the SAS studies. The solution of dMTO in methanol was dried under vacuum and the drug was re-dissolved in ultrapure water. The respective HSA solutions or $SEON^{LA\text{-}HSA}$ / $SEON^{LA\text{-}HSA*dMTO}$ suspensions were prepared as described in Section 2.3 and freeze-dried overnight. They were redispersed in the respective volume of H_2O. The solid content of the particle suspensions ranged from 0.01 wt. % to 1.28 wt. % ($m_{Particles}$ / $m_{Solvent}$). In the following sections the description "wt. %" shall describe this particular mass ratio. Samples with HSA were adjusted to the corresponding HSA amount in $SEON^{LA\text{-}HSA}$ according to the known core/shell ratio of 18% (m/m).

2.8 Small-angle neutron scattering (SANS)

SANS experiments were performed at KWS-1 SANS instrument of JCNS located at Heinz Maier-Leibnitz Zentrum (MLZ, Garching, Germany)[19,20]. The measurements were carried out at sample-to-detector distances of 1.5, 8 and 20 m using a non-polarized incident beam with a neutron wavelength of λ = 7 Å and wavelength spread of $\Delta\lambda/\lambda$ = 10%. The total covered *q*-range constituted 0.002 – 0.25 $Å^{-1}$. The samples were placed in 1 mm quartz cells and kept at room temperature. Corresponding H_2O/D_2O mixtures for background subtraction were measured along with the samples. A 1.5 mm thick flat piece of poly(methyl methacrylate) (PMMA) was used as a secondary absolute standard. Raw data were radially averaged and brought in absolute intensity units using QtiKWS10 software package [www.qtikws.de].

3. Results and Discussion

3.1 Adsorption of MTO to $SEON^0$, $SEON^{LA\text{-}HSA}$ and HSA

The adsorption equilibrium of MTO to the different compounds is displayed in Figure 1. Up to a concentration of 100 µg MTO / 2 mg iron (or the corresponding HSA concentration) MTO absorbs almost quantitatively to all compounds (above 94.8 ± 0.89%). The $SEON^0$ suspensions precipitated quickly after addition of MTO at concentrations of 250 µg/ml and above. The adsorption yield rapidly decreases to only 8.9 ± 0.25% at this concentration. We attribute this to reduction of surface area due to permanent agglomeration of the particles. This greatly decreases the number of possible interaction

sites with the drug. SEON^{LA-HSA} particles, which stayed colloidally stable even at the highest MTO concentration, show good binding capacity for MTO: 97.6% ± 0.06% of the drug is bound to the particles. Pure HSA solution showed a significant reduction in adsorption only at very high concentrations of 500 µg/ml MTO, where the adsorption yield was reduced to 94.7 ± 0.09%. These results confirm the hypothesis that the drug MTO has high binding to HSA as well as high binding to iron oxide surfaces. Which binding type is present in the hybrid material, however, cannot be concluded from such measurement.

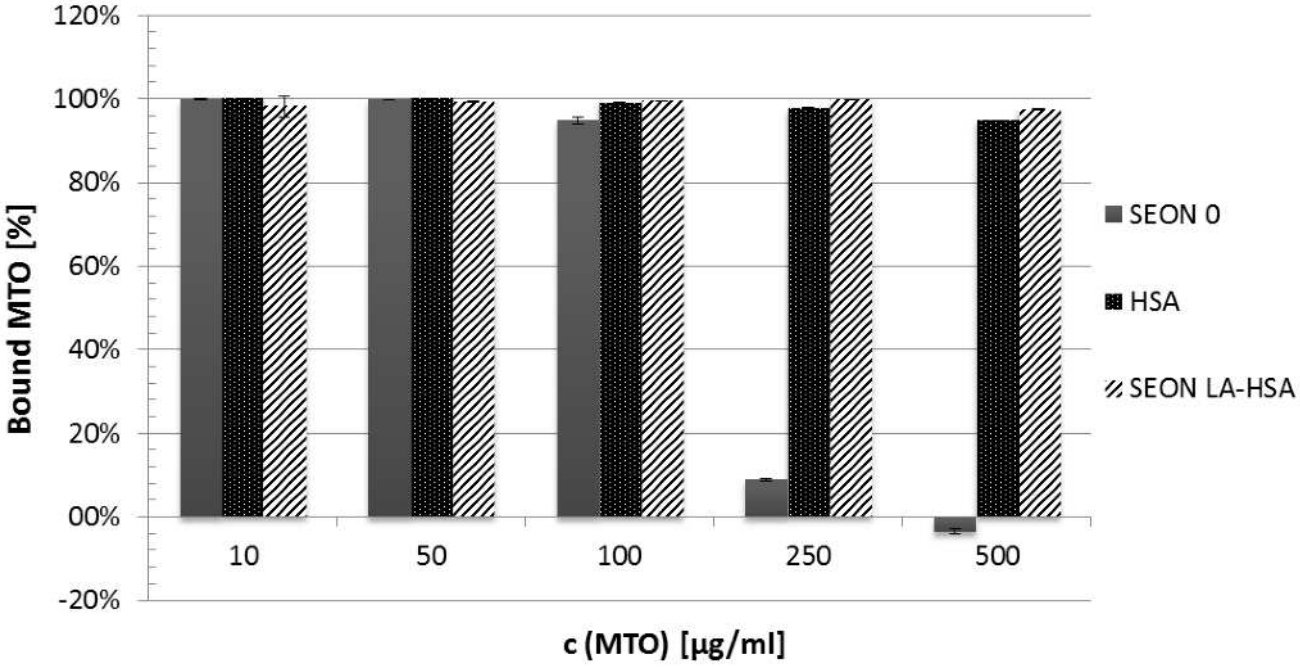

Figure 1. Amount of bound Mitoxantrone after adsorption to uncoated iron oxide nanoparticles (SEON^0), human serum albumin (HSA) and lauric acid/HSA coated iron oxide nanoparticles (SEON^{LA-HSA}). All measurements were performed in triplicates.

3.2 Desorption kinetics of MTO from SEON^0, SEON^{LA-HSA} and HSA

In accordance with previous results[11] the drug desorbed slowly from SEON^{LA-HSA} following a pseudo-zero-order kinetics. After 24 h, 30.3 ± 0.03 % of the original 300 µg had leaked into the dialysis medium (see Figure 2). Interestingly, the uncoated particles showed a similar linear desorption behavior. After 24 h 20.5 ± 0.14% of MTO were found in the medium. The binding of MTO to HSA proved to be less stable, a quick onslope allowed release of 49.5 ± 0.21% after 12 h. After that the release seemed to slow down, however, this could also be attributed to lack of sink conditions which is a commonly observed phenomenon in the dialysis bag assay[21]. Taken together, the coated particles displayed a desorption kinetics similar to the one of uncoated SEON^0 particles. Although the SEON^0 particles sediment quickly, the drug seemed to stay adsorbed to the particles. This is surprising, as the coagulation of the iron oxide cores seemed to influence the MTO binding capacity significantly in the static adsorption experiment. The release from HSA was much faster. Due to the fact that electrostatically adsorbed drug/particle complexes often display a quick burst release when they come

in contact with a medium with relatively high ionic strength[22] this could already indicate that the binding energy of MTO must be higher – or that a different binding mechanism is present. In an exemplary desorption assay using phosphate titration no desorption of MTO was observed (see supplementary Figure S8). The good binding of MTO to iron oxide nanoparticle surface has been shown before[23] and the present results could indicate that the binding energy of MTO to the $SEON^{LA\text{-}HSA}$ particles is similar to the binding energy of iron oxide surfaces ($SEON^{0}$) under the given conditions. However, albumin displays manifold different conformations depending on its chemical surroundings[24] and thus, it cannot be ruled out that HSA molecules which are presented on the surface of the particles are involved in the binding process.

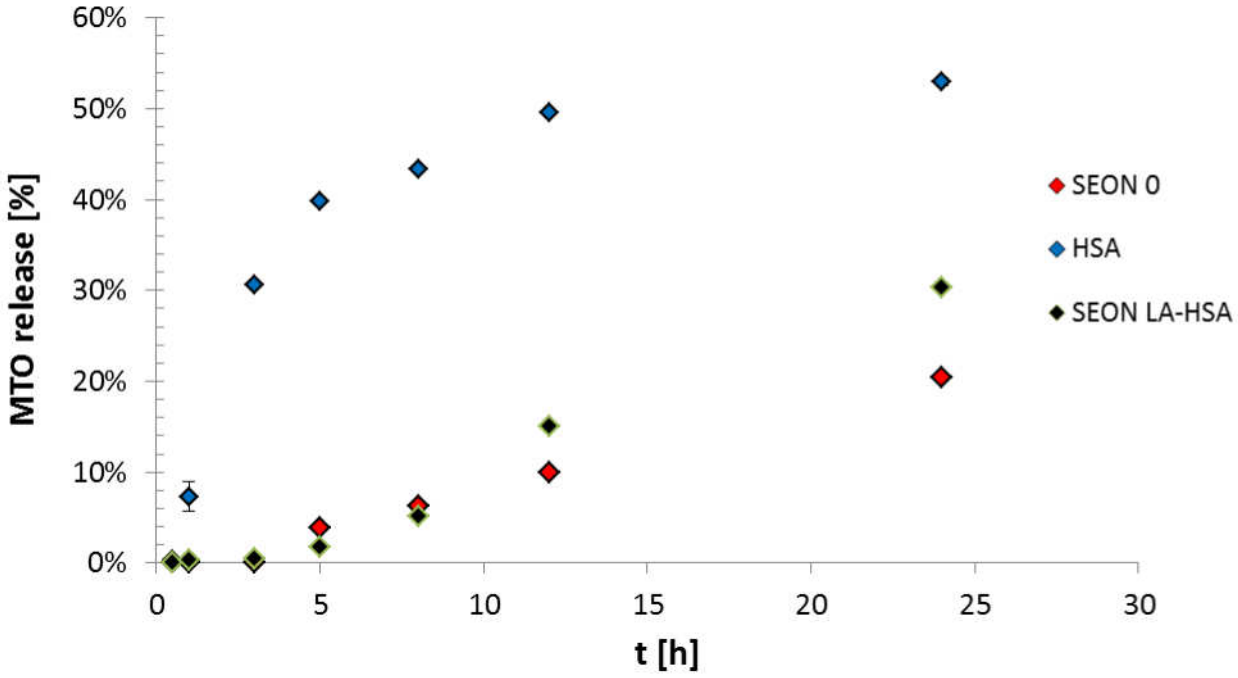

Figure 2. Desorption of MTO from $SEON^{0}$, HSA, and $SEON^{LA\text{-}HSA}$ in a dialysis model over time. All experiments were performed in duplicates.

3.3 Influence of MTO adsorption on $SEON^{LA\text{-}HSA}$ particles

It has been shown earlier that increasing amounts of commercial MTO solution (with salts) can have effects on colloidal stability of particles[11]. In order to understand the effect of MTO on the particle surface we used a salt-free solution for the adsorption studies in order to avoid salt effects. The results from DLS (Table 1) suggest a small reduction in hydrodynamic size and a narrower size distribution after MTO is added to the suspension. This could indicate a change in interaction between the particles. Self-assembly of nanoparticles is a very complex phenomenon and depends on various parameters including particle size, interparticle distance, the composition of the dispersion medium, and, as discussed before, the particle surfaces[25]. Broadening of the size distribution could therefore indicate changes in any of the aforementioned characteristics, causing the particles to arrange differently. However, neither the differences in size nor the differences in the distribution width are statistically significant and therefore cannot serve as a proof of changes in particle interaction. Using

surface analysis and small-angle scattering techniques we therefore tried to investigate this effect further.

In order to better understand the particle interactions and the effect of drug binding on the colloid we also investigated the surface charge in a dynamic model as function of the pH or an oppositely charged polymer. As can be seen in Figure 3A, both samples show similar pH-dependence of the surface charge with a good correlation to what has been described before about such hybrid coated systems[26]. The isoelectric points of the colloids, which was calculated from the fits, was 5.10 ± 0.07 for $SEON^{LA-HSA}$ and 5.08 ± 0.07 for $SEON^{LA-HSA*MTO}$. This small and statistically insignificant difference (in a paired, two-sided student's T-test) shows that the pH-dependent surface chemistry of the colloid is not greatly affected by the binding of MTO. Changes in pH-dependent surface chemistry can indicate binding of new molecules or presentation of different functional groups to or on particle surfaces[27]. However, measurement of absolute charges by titrating Zeta potential of particles at constant pH can provide further insight into surface adsorption phenomena.

Polyelectrolyte titration allows estimation of the surface charges of a colloid at a constant particle concentration, pH and ionic strength of the dispersion medium[28,29]. Under well-defined conditions particles with or without MTO display similar surface charge (Figure 3B). The zero of the linear fits were calculated as n = 0.1239 µmol for the MTO loaded particles and n = 0.1244 µmol for the native particles, respectively. Although this amount is a merely artificial value, the result confirms that the surface charges of the two investigated systems are almost similar. However, the small but statistically significant (p<0.05) difference in charge at the beginning of the titration may indicate differences in the surfaces. By MTO adsorption the zeta potential of the $SEON^{LA-HSA}$ particles decreases from −36.3 ± 2.5 mV to −31.5 ± 1.4 mV. MTO has shown to reduce the absolute value of the zeta potential of iron oxide nanoparticles before[26]. The fact that this difference disappears during surface titration could indicate that Poly(DADMAC) possesses higher affinity to the surface than the drug, and therefore displaces MTO from the surface.

Table 1. DLS data for $SEON^{LA-HSA}$ and $SEON^{LA-HSA*MTO}$. Mean hydrodynamic size was calculated as surface mean diameter (SMD). All experiments were performed in triplicates.

	$SEON^{LA-HSA}$	$SEON^{LA-HSA*MTO}$
Hydrodynamic diameter [nm]	59.2 ± 0.3	58.8 ± 0.4
Polydispersity of Gaussian fit [a.u.]	0.34 ± 0.03	0.31 ± 0.01

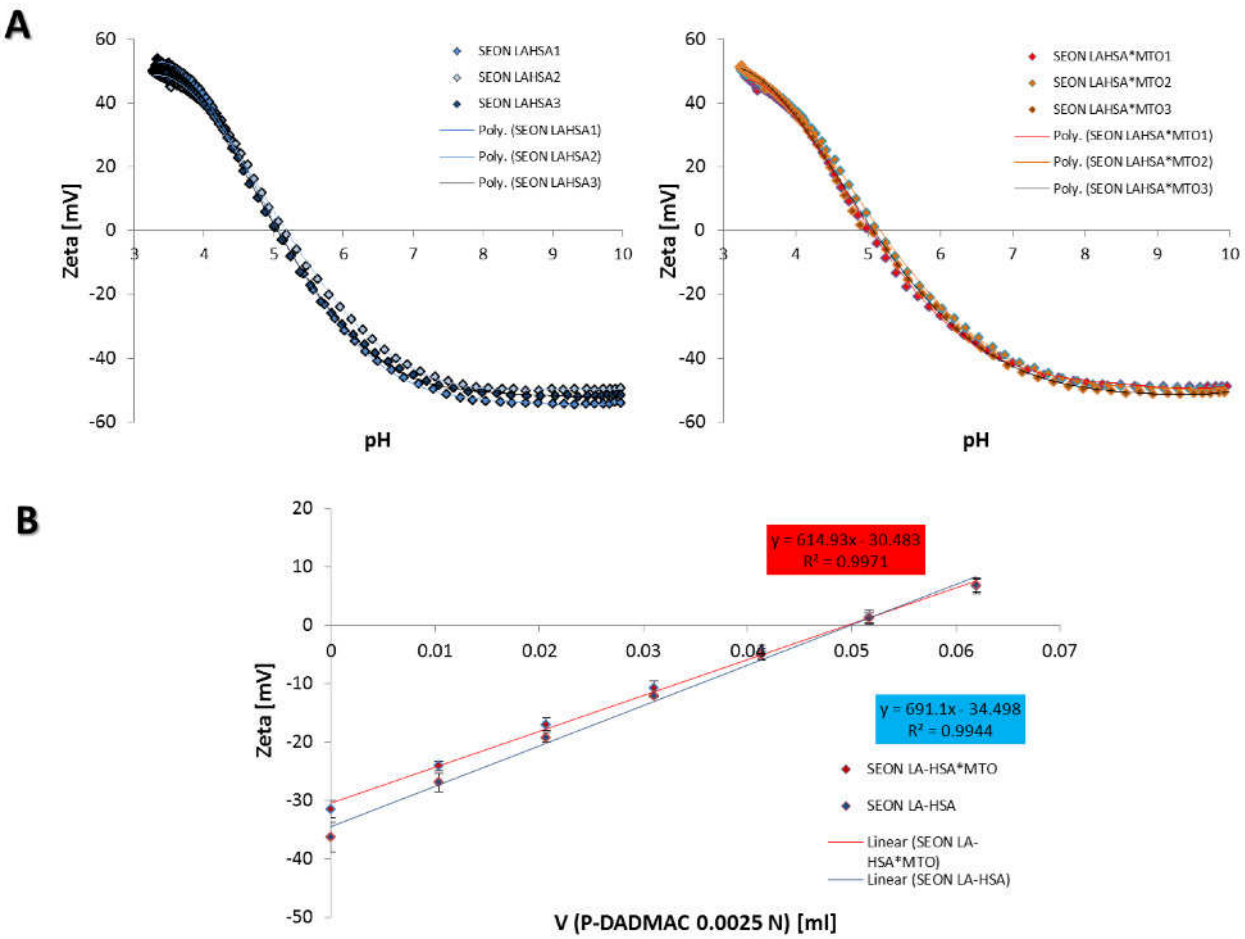

Figure 3. (A) pH-dependent surface titration of SEON$^{LA\text{-}HSA}$ and SEON$^{LA\text{-}HSA*MTO}$ with polynomic fits. Titrations were performed on n=3 individual samples. (B) Surface charge titration of SEON$^{LA\text{-}HSA}$ and SEON$^{LA\text{-}HSA*MTO}$ at pH 7.40. Values are displayed as mean and standard deviation of n=3 titrations.

3.4 SAS studies

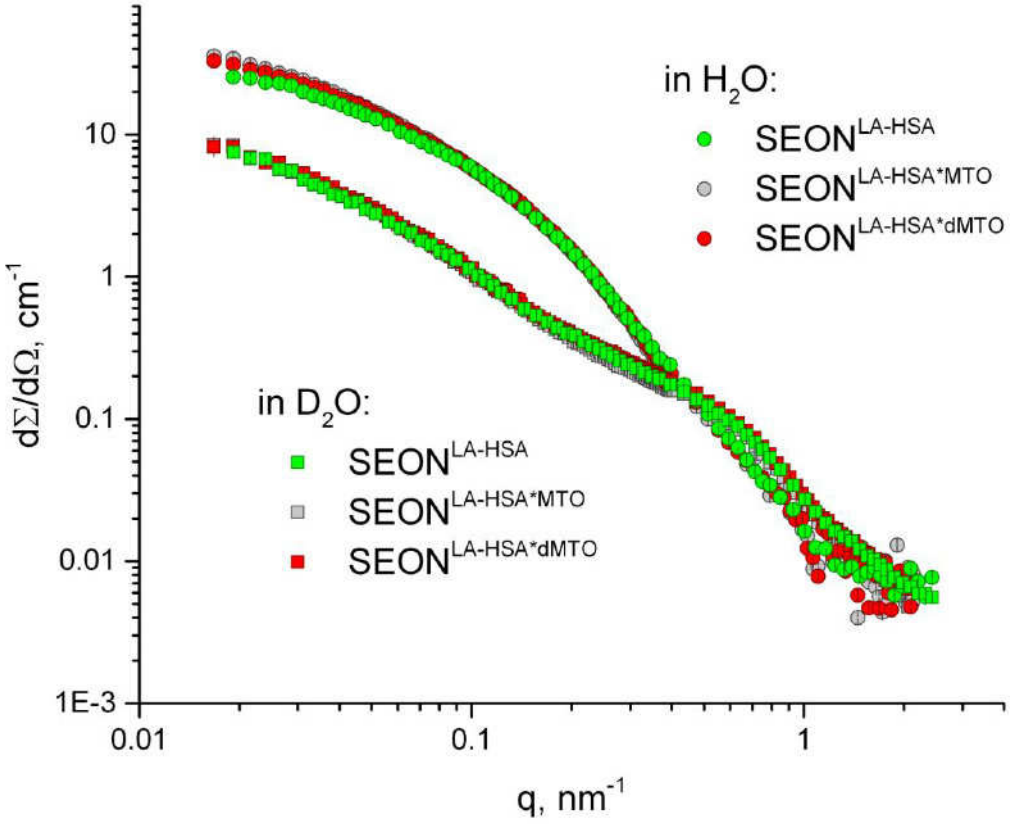

Figure 4. SANS scattering curves of the initial SEON^{LA-HSA} at 1.28 wt. % magnetic nanoparticles and after the addition of MTO and dMTO (in two limiting contrast conditions, namely H_2O- and D_2O-based solvents). 100 µg/ml of MTO drug has been added into the initial SEON^{LA-HSA} system.

Small-angle neutron scattering measurements have been performed to visualize the location of MTO after adsorption to SEON^{LA-HSA} by measurements in H_2O and D_2O using MTO and dMTO (Figure 4). The initial SEON^{LA-HSA} suspensions have been measured too (Figure 4). Expected neutron scattering length densities for components are represented in supplementary Table S1. The scattering intensity is proportional to the squared difference in scattering length densities ($\Delta\rho^2$, the so called contrast). In SANS case, according to supplementary Table S1, in H_2O the iron oxide cores and dMTO should give the most dominant contributions and in D_2O-based solvent the LA-HSA and MTO should be the main contributors to the scattering signal. Significant fraction of compact distribution of MTO will produce visible changes in scattering curves of MTO and dMTO and integral scattering parameter such as the radius of gyration (R_g). The R_g value is the average of square center-of-mass distances in the particle weighted by the scattering length density and thus the R_g reflects the particle's size[30]. As one can see the scattering intensities in Figure 4 change insignificantly which points on very small fraction of MTO in SEON^{LA-HSA} and/or non-aggregated state of MTO molecules within SEON^{LA-HSA}. We attribute the slight difference visible in the scattering intensities between the initial system and after the drug addition in H_2O-based samples to the difference in the prepared SPIONs batches. The similarity of the

scattering curves from D_2O-based samples lets us make an assumption that MTO adsorbs as a separate molecule and does not aggregate into supramolecular complexes.
SANS measurements point to the negligible contribution of MTO in total scattering from the $SEON^{LA-HSA*MTO}$ system. According to Section 3.1, the MTO drug adsorbs very well to $SEON^{LA-HSA}$. As $SEON^{LA-HSA}$ consists of multicore clusters (see supplementary Figure S6) the arising question is whether it gets incorporated inside the nanoparticles (iron oxide/LA-HSA interface) or stays on outer surface of LA-HSA coating. Each location of MTO should be reflected in the scattering of the whole particle system. MTO at outer surface of LA-HSA coating should change the interaction of $SEON^{LA-HSA*MTO}$ particles with each other compared to $SEON^{LA-HSA}$ and MTO at iron oxide/LA-HSA interface shouldn't.
We applied SAXS technique, which is beneficial by its faster measurement time, better statistics and lower background, which, on the contrary, becomes significant in SANS due to the incoherent scattering from hydrogen present in high amounts in bio-macromolecules. Moreover, in SAXS the contrast of iron oxide nanoparticles is much higher than that of LA, HSA and MTO (see supplementary Table S1) and thus the scattering signal in SAXS is originated from the iron oxide only and the interaction between nanoparticles in $SEON^{LA-HSA}$ and $SEON^{LA-HSA*MTO}$ can be probed.

The whole set of scattering curves was obtained for concentrations from 0.01 to 1.28 wt. % of magnetic nanoparticles. As mentioned above the scattering signal can be fully attributed to the iron oxide part of nanoparticles (their clusters). The SAXS scattering curves repeat the behavior of the SANS scattering curves in H_2O (compare Figure 4 and supplementary Figure S3). A possible interparticle interaction would influence the initial slope of the scattering curve (lowest q-range)[32]. The comparison of the SAXS scattering curves for the 1.28 wt. % concentration before and after the drug addition can be found in supplementary Figure S4. The initial slopes of the scattering curves are different (interaction among particles changed) and SAXS curves have higher intensity in the low-q range after the addition of the drug.
Moreover, we used the fact that the SAXS scattering curve at lowest concentration (0.01 wt. %) is almost free of any interparticle interaction and obtained the structure factor by dividing the SAXS curve from the most concentrated sample (1.28 wt. %) by the lowest concentration (0.01%).
In the case of interactive system the SAXS intensity, $I(q)$, can be written in the simplified way as

$$I(q)=n\cdot P(q)\cdot S(q), \quad (2)$$

where n is particle concentration, $P(q)$ is particle's scattering form factor, which includes size, shape and contrast of the particles, and $S(q)$ is the structure factor, which represents interparticle interaction. At very low concentration the $S(q)$ is equal to 1. At high concentrations in case of attraction among the particles the $S(q)$ is larger than 1 for the lowest q-range and smaller than 1 in case of repulsive interaction[31,32]. Thus it is possible to get the indication on type of $S(q)$ function and its change depending on system variation by dividing the scattering curves for the highest concentration to that of the smallest.

The resulting structure factors are represented in Figure 5. The structure factor at lower q decreases slower after the drug addition, which points out to the reduction of the interparticle repulsive

interaction in the system. In the case of charged particles such as in SEON^{LA-HSA} it could be due to the decrease of Debye screening length (increase of free ions in solution) or due to the adsorption of drug on the surface of SEON^{LA-HSA} particles (with the reduction of surface charge).

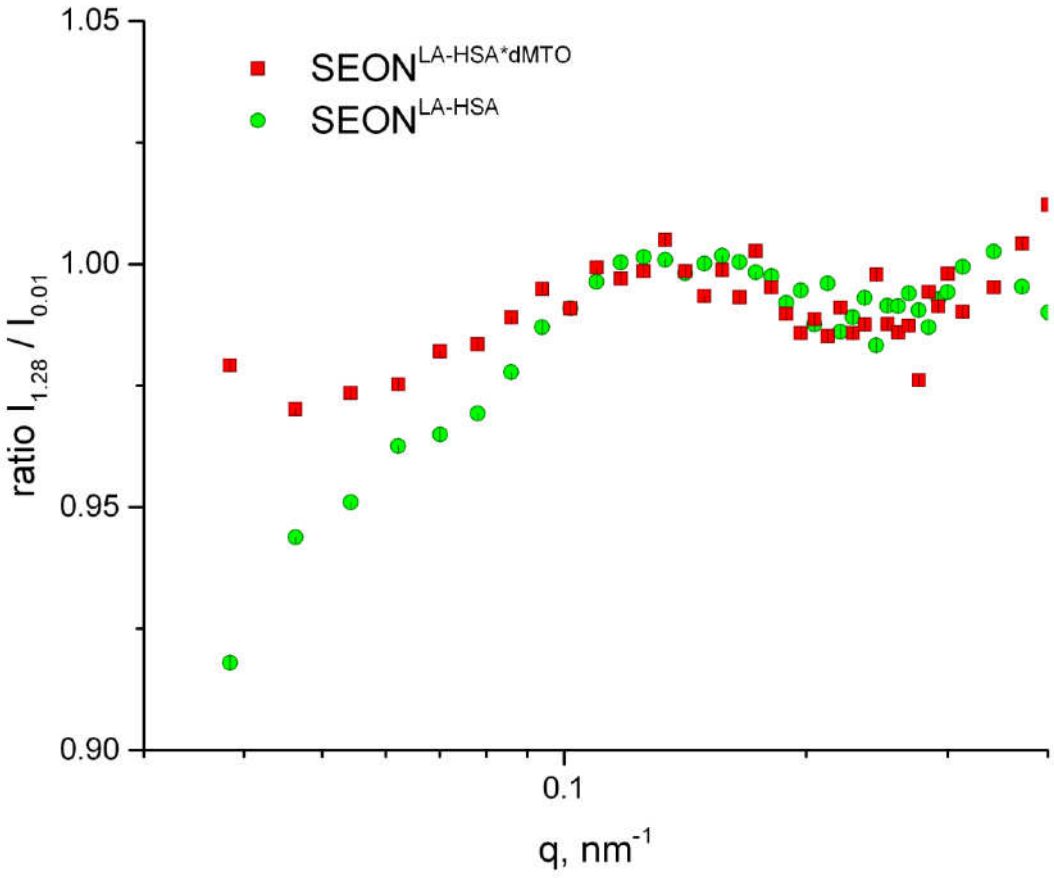

Figure 5. Structure factor experimentally determined as a ratio between SAXS curves at 1.28 (highest concentration) and 0.01 wt. % (highest dilution) content of magnetic nanoparticles for sample before and after the addition of dMTO. The structure factors were normalized on sample concentration. Low-*q* range is represented. The difference between the structure factors in the low-*q* region points to the reduction of interaction in the system after the drug addition.

To check the effect of possible free salts on interaction in the samples (Debye screening length variation), the amount of residual salts in SEON^{LA-HSA} and SEON$^{LA-HSA*dMTO}$ was estimated and constituted 5.00 and 5.03 mM, respectively. These values correspond to the Debye screening lengths of 4.287 and 4.274 nm. Taking this into account we estimated how much would the excluded volume of the nanoclusters change if one considers an increase in their size due to the Debye length (a rough cluster size estimation has been done by the indirect Fourier transformation approach[33] and gives an average radius of 39 nm if we assume clusters of nanoparticles of spherical shape (see Supporting Information)). The factor for the volume increase would thus increase by 1.367 and 1.366 for SEON^{LA-HSA} and SEON$^{LA-HSA*dMTO}$, respectively. The difference of less than 0.07% points to the fact that such a small difference in free salt concentrations in the samples would not lead to the observed effect in

Figure 5. With this we conclude that the obtained distinction of structure factor in small q for the SEON$^{\text{LA-HSA*dMTO}}$ sample is due to the adsorption of the MTO drug onto SEON$^{\text{LA-HSA}}$.

SANS and SAXS on SEON$^{\text{LA-HSA*dMTO}}$ suggest that the dMTO decreases the interaction between clusters i.e., it should be located at the outer shell of SEON$^{\text{LA-HSA}}$ clusters (namely at the LA-HSA layer) and there should occur a molecular adsorption of dMTO. That is why the interaction between LA-HSA and dMTO has been studied by SAXS in mixtures of LA-HSA and LA-HSA with dMTO (100 µg/ml) with the amounts of constituents corresponded to the SEON$^{\text{LA-HSA}}$ sample with magnetic nanoparticles. SAXS curves obtained from the LA-HSA and LA-HSA*dMTO samples were fitted with the model of an oblate ellipsoid of revolution (corresponding to HSA molecule shape[33]) with the screened Coulomb interaction[34] using SasView 4.1 package[36].

The ratios of the volume fractions inside the LA-HSA and LA-HSA*dMTO series, as well as between them, were fixed during the fit. The surface charge was fitted assuming it to be constant within the certain sample series. Parameters of the intensity scale and semi-axes of the ellipsoid were globally fixed (we used the small-angle scattering data at low concentrations to determine the semi-axis of the model ellipsoid, where the interparticle interaction can be neglected). Increase of the surface charge tends to shift the interaction peak to the smaller q and increases its amplitude, whereas an increase in the sample volume fraction tends to shift the peak to the region of larger q. Fixing the relation between sample concentrations let us unambiguously determine the average surface charge in the sample series. The free salt content parameter, which mostly influences the smallest q was fitted independently for each sample concentration and was kept to be close for the LA-HSA and LA-HSA*dMTO samples of the same concentrations. The results of the fit are represent in the Figure 6 and in Table 2.

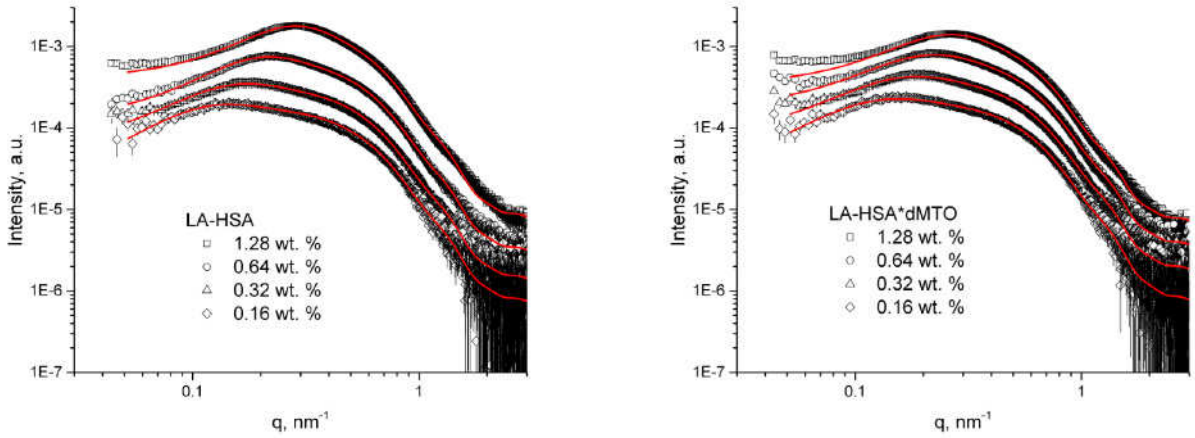

Figure 6. The SAXS scattering curves of LA-HSA and LA-HSA*dMTO series together with the fits to the model of oblate ellipsoid of revolution with the screened Coulomb interaction. Amount of the lauric acid and human serum albumin corresponds to that of the initial SEON$^{\text{LA-HSA}}$ samples (indicated in the legend).

For both samples the model ellipsoid semi-axes of 1.76 nm (polar) and 4.7 nm (equatorial) were obtained, which is in agreement with Zhang *et al*[35]. At the same time the average surface charge of the particles obtained from the fit is lower for the sample with the drug (see Table 2). This is in full agreement with the results obtained from the analysis of the experimentally determined structure factor

and allows us to make a conclusion about the reduction of interaction in LA-HSA complex after dMTO addition.

Table 2. Structural parameters and surface charge as obtained from fits of the SAXS data.

Sample	Polar radius	Equatorial radius	Charge
LA-HSA	1.76 ±0.04 nm	4.70 ± 0.03 nm	13.4 ± 0.2 *e*
LA-HSA*dMTO			11.8 ± 0.1 *e*

Addition of dMTO leads to decreasing of charge values of LA-HSA complex, which suggests affinity between LA-HSA and dMTO and supports behavior of $SEON^{LA\text{-}HSA*dMTO}$ in small-*q* region. This may be attributed to the location of dMTO at the outer shell of LA-HSA complex, which is also in concordance with the results from polyelectrolyte titrations.

4. Conclusions

The adsorption/desorption and titration studies confirmed the original hypothesis that MTO possesses strong adsorption to naked iron oxide surface, naked HSA and the LA-HSA coated particles ($SEON^{LA\text{-}HSA}$) altogether. At the concentrations which we tested in FTIR, desorption, titration and SAS by neutrons and X-rays we can therefore safely assume that the drug is bound to the particles almost quantitatively. FTIR study and the pH-dependent Zeta potential analysis confirm the presence of LA-HSA on the particle surface, which is also in concordance with earlier results[11]. However, due to the low n/n ratio of functional groups the MTO is undetectable by FTIR. The release of the drug from the particles, which can provide information about the strength of the binding[36] is significantly slower compared to the release from pure albumin. The absence of burst release further underlines the stability of the binding even in media with high ionic strength. Surface titration experiments showed that on the one hand the addition of MTO did not alter the surface properties as far as absolute charge and pH-dependence of charge are concerned. However, presence of MTO caused a reduction of the particle's zeta potential which was eliminated during titration with high-affinity polymer Poly(DADMAC). This may suggest a displacement of drug due to elimination of charged surface on the outer shell of particles. Small molecules with high affinity towards iron oxides like phosphate, however, are not able to remove MTO from the particle surface. Taken together, this leads to the conjecture that surface charges on the outer shell play a role in the interaction mechanism of MTO and $SEON^{LA\text{-}HSA}$ particles.

SANS contrast variation showed that the initial $SEON^{LA\text{-}HSA}$ system consists of multicore particle aggregates, which have an organic shell. According to SANS data on deuterated and protonated MTO the adsorption of MTO takes place in form of separated molecules (there is no supramolecular aggregation of MTO). Complementary SAXS studies of the $SEON^{LA\text{-}HSA}$ concentration series together with the separate SAXS studies of the mixture of LA-HSA before and after the addition of dMTO showed the reduction of repulsive interaction between the particles. $SEON^{LA\text{-}HSA*dMTO}$ and decreasing of electrical charge of LA-HSA complex. Location of dMTO at the outer surface of $SEON^{LA\text{-}HSA*dMTO}$ gives the reduction of electrical potential and decreasing repulsion among SPIONs particles.

Taken together, these results show that the addition of MTO to the $SEON^{LA-HSA}$ system leads to a reduction in the interaction of its cluster, which is most likely due to a compensation of surface charge. This leads to a change in cluster-cluster interaction, which is also in concordance with earlier findings which confirmed destabilization of $SEON^{LA-HSA}$ by MTO[11]. Most likely the drug is located on the outer organic shell through the electrostatic adsorption. Location of MTO molecules at surface of $SEON^{LA-HSA}$ should be considered for further application of such formulations.

Acknowledgments

This study was supported by the DFG (AL552/5-2, TR408/4-3 and OD18/23-1), the Else Kröner-Fresenius Stiftung (Bad Homburg v. d. H.) and the EU project FP7-NMP-2012-LARGE-6-309820 "NanoAthero". The excellent support of Dr. Clement Blanchet (EMBL) and the staff of PETRA III during SAXS measurements is kindly acknowledged. This work benefited from the use of the SasView application, originally developed under NSF award DMR-0520547. SasView contains code developed with funding from the European Union's Horizon 2020 research and innovation programme under the SINE2020 project, grant agreement No 654000. This work is based upon experiments performed at the KWS-1 instrument operated by the Jülich Centre for Neutron Science (JCNS) at the Heinz Maier-Leibnitz Zentrum (MLZ), Garching, Germany.

Conflicts of Interest

The authors declare no conflict of interest.

References

1. Gobbo OL, Sjaastad K, Radomski MW, Volkov Y, Prina-Mello A. Magnetic Nanoparticles in Cancer Theranostics. *Theranostics.* 07/15/accepted 2015;5(11):1249-1263.

2. Lyer S, Tietze R, Unterweger H, et al. Nanomedical innovation: the SEON-concept for an improved cancer therapy with magnetic nanoparticles. *Nanomedicine (London, England).* Nov 2015;10(21):3287-3304.

3. Tietze R, Lyer S, Durr S, et al. Efficient drug-delivery using magnetic nanoparticles--biodistribution and therapeutic effects in tumour bearing rabbits. *Nanomedicine : nanotechnology, biology, and medicine.* Oct 2013;9(7):961-971.

4. Wahajuddin, Arora S. Superparamagnetic iron oxide nanoparticles: magnetic nanoplatforms as drug carriers. *International journal of nanomedicine.* 2012;7:3445-3471.

5. Tombacz E, Turcu R, Socoliuc V, Vekas L. Magnetic iron oxide nanoparticles: Recent trends in design and synthesis of magnetoresponsive nanosystems. *Biochemical and biophysical research communications.* Dec 18 2015;468(3):442-453.

6. Alexiou C, Tietze R, Schreiber E, et al. Cancer therapy with drug loaded magnetic nanoparticles—magnetic drug targeting. *J Magn Magn Mater.* 5// 2011;323(10):1404-1407.

7. Laurent S, Forge D, Port M, et al. Magnetic iron oxide nanoparticles: synthesis, stabilization, vectorization, physicochemical characterizations, and biological applications. *Chemical reviews.* Jun 2008;108(6):2064-2110.

8. Lourenco C, Teixeira M, Simões S, Gaspar R. Steric stabilization of nanoparticles: Size and surface properties. *International journal of pharmaceutics.* 1996/07/12 1996;138(1):1-12.

9. Friedrich RP, Zaloga J, Schreiber E, et al. Tissue Plasminogen Activator Binding to Superparamagnetic Iron Oxide Nanoparticle-Covalent Versus Adsorptive Approach. *Nanoscale research letters.* Dec 2016;11(1):297.

10. Ulbrich K, Holá K, Šubr V, Bakandritsos A, Tuček J, Zbořil R. Targeted Drug Delivery with Polymers and Magnetic Nanoparticles: Covalent and Noncovalent Approaches, Release Control, and Clinical Studies. *Chemical reviews.* 2016/05/11 2016;116(9):5338-5431.

11. Zaloga J, Pottler M, Leitinger G, et al. Pharmaceutical formulation of HSA hybrid coated iron oxide nanoparticles for magnetic drug targeting. *European journal of pharmaceutics and biopharmaceutics : official journal of Arbeitsgemeinschaft fur Pharmazeutische Verfahrenstechnik e.V.* Feb 8 2016.

12. Wishart DS, Knox C, Guo AC, et al. DrugBank: a comprehensive resource for in silico drug discovery and exploration. *Nucleic acids research.* Jan 1 2006;34(Database issue):D668-672.

13. Khan SN, Islam B, Yennamalli R, Sultan A, Subbarao N, Khan AU. Interaction of mitoxantrone with human serum albumin: Spectroscopic and molecular modeling studies. *European Journal of Pharmaceutical Sciences.* 12/18/ 2008;35(5):371-382.

14. Herman EH, Zhang J, Hasinoff BB, Clark JR, Jr., Ferrans VJ. Comparison of the structural changes induced by doxorubicin and mitoxantrone in the heart, kidney and intestine and characterization of the Fe(III)-mitoxantrone complex. *Journal of molecular and cellular cardiology.* Sep 1997;29(9):2415-2430.

15. Zaloga J, Stapf M, Nowak J, et al. Tangential Flow Ultrafiltration Allows Purification and Concentration of Lauric Acid-/Albumin-Coated Particles for Improved Magnetic Treatment. *International journal of molecular sciences.* 2015;16(8):19291-19307.

16. Hamilton JA. Medium-chain fatty acid binding to albumin and transfer to phospholipid bilayers. *Proceedings of the National Academy of Sciences of the United States of America.* 1989;86(8):2663-2667.

17. Tietze R, Schreiber E, Lyer S, Alexiou C. Mitoxantrone loaded superparamagnetic nanoparticles for drug targeting: a versatile and sensitive method for quantification of drug enrichment in rabbit tissues using HPLC-UV. *Journal of biomedicine & biotechnology.* 2010;2010:597304.

18. Franke D, Kikhney AG, Svergun DI. Automated acquisition and analysis of small angle X-ray scattering data. *Nuclear Instruments and Methods in Physics Research Section A: Accelerators, Spectrometers, Detectors and Associated Equipment.* 10/11/ 2012;689:52-59.

19. Feoktystov AV, Frielinghaus H, Di Z, et al. KWS-1 high-resolution small-angle neutron scattering instrument at JCNS: current state. *Journal of Applied Crystallography.* 2015;48(1):61-70.

20. Heinz-Maier-Leibnitz-Zentrum. KWS-1: Small-angle scattering diffractometer. *Journal of large-scale research facilities.* Vol (1)2015.

21. Modi S, Anderson BD. Determination of drug release kinetics from nanoparticles: overcoming pitfalls of the dynamic dialysis method. *Molecular pharmaceutics.* Aug 5 2013;10(8):3076-3089.

22. Manocha B, Margaritis A. Controlled Release of Doxorubicin from Doxorubicin/-Polyglutamic Acid Ionic Complex. *Journal of Nanomaterials.* 2010;2010:9.

23. Tietze R, Schreiber E, Lyer S, Alexiou C. Mitoxantrone Loaded Superparamagnetic Nanoparticles for Drug Targeting: A Versatile and Sensitive Method for Quantification of Drug Enrichment in Rabbit Tissues Using HPLC-UV. *Journal of Biomedicine and Biotechnology.* 2010;2010:8.

24. Shang L, Wang Y, Jiang J, Dong S. pH-Dependent Protein Conformational Changes in Albumin:Gold Nanoparticle Bioconjugates: A Spectroscopic Study. *Langmuir : the ACS journal of surfaces and colloids.* 2007/02/01 2007;23(5):2714-2721.

25. Bishop KJM, Wilmer CE, Soh S, Grzybowski BA. Nanoscale Forces and Their Uses in Self-Assembly. *Small.* 2009;5(14):1600-1630.

26. Zaloga J, Janko C, Nowak J, et al. Development of a lauric acid/albumin hybrid iron oxide nanoparticle system with improved biocompatibility. *International journal of nanomedicine.* 2014;9:4847-4866.

27. van Rijt SH, Bölükbas DA, Argyo C, et al. Protease-Mediated Release of Chemotherapeutics from Mesoporous Silica Nanoparticles to ex Vivo Human and Mouse Lung Tumors. *ACS nano.* 2015/03/24 2015;9(3):2377-2389.

28. Häuser M, Langer K, Schönhoff M. pH-Triggered release from surface-modified poly(lactic-co-glycolic acid) nanoparticles. *Beilstein journal of nanotechnology.* 12/11/accepted 2015;6:2504-2512.

29. Illés E, Tombácz E. The effect of humic acid adsorption on pH-dependent surface charging and aggregation of magnetite nanoparticles. *Journal of colloid and interface science.* 3/1/ 2006;295(1):115-123.

30. Guinier A, Fournet G. *Small-Angle Scattering of X-Rays.* New York: Wiley; 1955.

31. Kaler EW. Small angle scattering from complex fluids. *Modern Aspect of Small Angle Scattering*. Netherlands1997:329-353.

32. Pedersen JS. Analysis of small-angle scattering data from colloids and polymer solutions: modeling and least-squares fitting. *Adv Colloid Interfac.* Jul 18 1997;70:171-210.

33. Fukasawa T, Sato T. Versatile application of indirect Fourier transformation to structure factor analysis: from X-ray diffraction of molecular liquids to small angle scattering of protein solutions. *Physical Chemistry Chemical Physics.* 2011;13(8):3187-3196.

34. Hayter JB, Penfold J. An analytic structure factor for macroion solutions. *Molecular Physics.* 1981/01/01 1981;42(1):109-118.

35. Zhang F, Skoda MWA, Jacobs RMJ, Martin RA, Martin CM, Schreiber F. Protein Interactions Studied by SAXS: Effect of Ionic Strength and Protein Concentration for BSA in Aqueous Solutions. *The Journal of Physical Chemistry B.* 2007/01/01 2007;111(1):251-259.

36. Vulic K, Shoichet MS. Affinity-based drug delivery systems for tissue repair and regeneration. *Biomacromolecules.* Nov 10 2014;15(11):3867-3880.

37. Glatter OK, O. *Small-angle X-ray Scattering.* London: Academic Press; 1982.

38. Ang JC, Henderson MJ, Campbell RA, et al. Human serum albumin binding to silica nanoparticles--effect of protein fatty acid ligand. *Physical chemistry chemical physics : PCCP.* Jun 07 2014;16(21):10157-10168.

39. Stuhrmann H. Neutron small-angle scattering of biological macromolecules in solution. *Journal of Applied Crystallography.* 1974;7(2):173-178.

40. Avdeev MV, Feoktystov AV, Kopcansky P, et al. Structure of water-based ferrofluids with sodium oleate and polyethylene glycol stabilization by small-angle neutron scattering: contrast-variation experiments. *Journal of Applied Crystallography.* 2010;43(5 Part 1):959-969.

41. Glatter O. New Method for Evaluation of Small-Angle Scattering Data. *J Appl Crystallogr.* 1977;10(Oct1):415-421.

Supplementary Information

SANS contrast variation on $SEON^{LA\text{-}HSA}$

The contrast variation experiment revealed a complex structural organization of the $SEON^{LA\text{-}HSA}$ particles with rather large objects in the system (Figure S1).

The organic shell of the $SEON^{LA\text{-}HSA}$ particles contributes the most in the D_2O-based sample (100% D_2O curve in Figure S1). Its scattering intensity consists of two contributions: large objects at $q < 0.2$ nm^{-1} and free molecules of HSA at $q > 0.2$ nm^{-1}. The power-law dependence of the initial part of the curve has an exponent of −1.2, which is close to the case of elongated objects[37]. If one compares the scattering curves for 0% D_2O (i.e. H_2O) and 100% D_2O, then one can see that 100% D_2O curve is much steeper, which points to a conclusion that the structures responsible for "lite" components visible in D_2O (Table S1) are much larger than structures which are observed in H_2O-based sample (mainly iron oxide clusters).

Table S1. Scattering length densities (in units $\times 10^{10}$ cm^{-2}) of different components and their contrasts (in units $\times 10^{20}$ cm^{-4}) in H_2O- and D_2O-based solvents (density of MTO and dMTO were considered be 0.88 and 0.9 g/cm^3, respectively).

	SLD/contrast	Compound						
		H_2O	D_2O	Iron oxide	LA	HSA*	MTO	dMTO
Neutrons	ρ	−0.56	6.33	6.97	0.04	1.66	~1.36	~2.36
	$\Delta\rho^2$ in H_2O			56.7	0.36	4.93	3.69	8.53
	$\Delta\rho^2$ in D_2O			0.41	39.6	21.81	24.7	15.8
X-rays	ρ	9.47	9.37	40.7	8.37	12.1	~7.96	~7.99
	$\Delta\rho^2$ in H_2O			975.3	1.21	6.92	2.28	2.19
	$\Delta\rho^2$ in D_2O			981.6	1	7.45	1.99	1.9

* from Ref. No[38]

The scattering intensity has a quadratic dependence on the contrast in the system[39] and its minimum at $q \to 0$, the so-called match point, gives an average particle SLD. But in our case the regular approach of Guinier approximation in order to obtain a dependence of $I(q \to 0)$ on D_2O content in the solvent becomes impossible due to the large aggregates. Nevertheless, here we have built a dependence of the match point on the q-value. Such dependence sheds light on the internal organization of the detected large structures in the samples [40]. In our case the dependence is similar to the one reported by Avdeev *et al*[40], which indicates the existence of close to homogenous clusters in the system (Figure S2).

Thus, we can conclude that the $SEON^{LA\text{-}HSA}$ system consists of elongated close to homogeneous aggregates with outer organic shell and free molecules of HSA in the solvent.

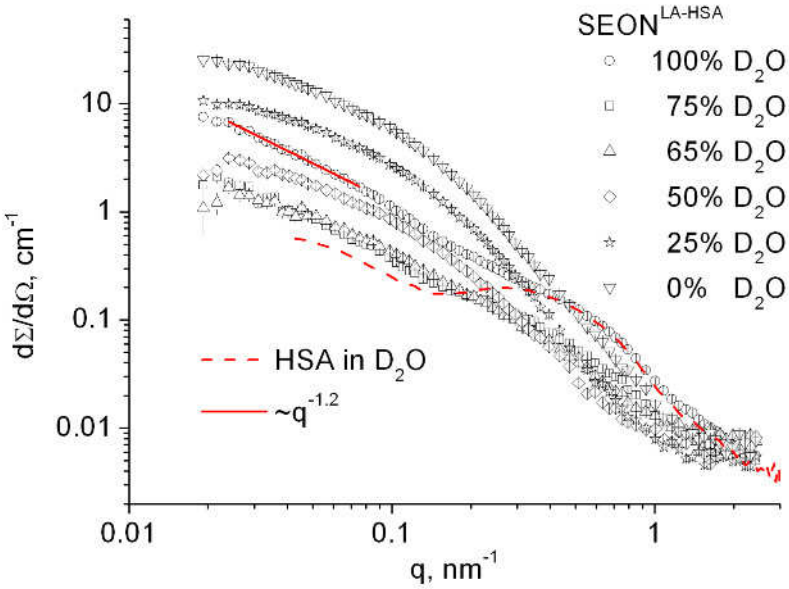

Figure S1. SANS scattering curves for the contrast variation series on SEON$^{LA\text{-}HSA}$ system. The D_2O content in the solvent is indicated in the legend. HSA scattering curve (dashed line; scaled) is compared with the scattering curve of 100% D_2O. Approximation of the initial part of the 100% D_2O scattering curve is of a power-law type with an exponent of −1.2 (solid line).

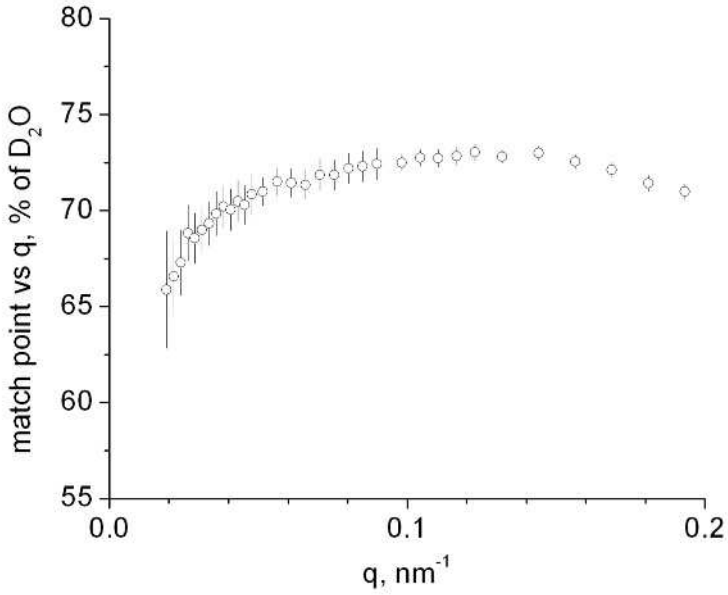

Figure S2. Dependence of the effective match point on *q*. The behavior of the curve indicates a close to homogeneous clusters in the system (slight SLD variation with *q*, i.e. real apparent size).

SAXS on SEON$^{LA\text{-}HSA}$ *and* SEON$^{LA\text{-}HSA*dMTO}$ *systems*

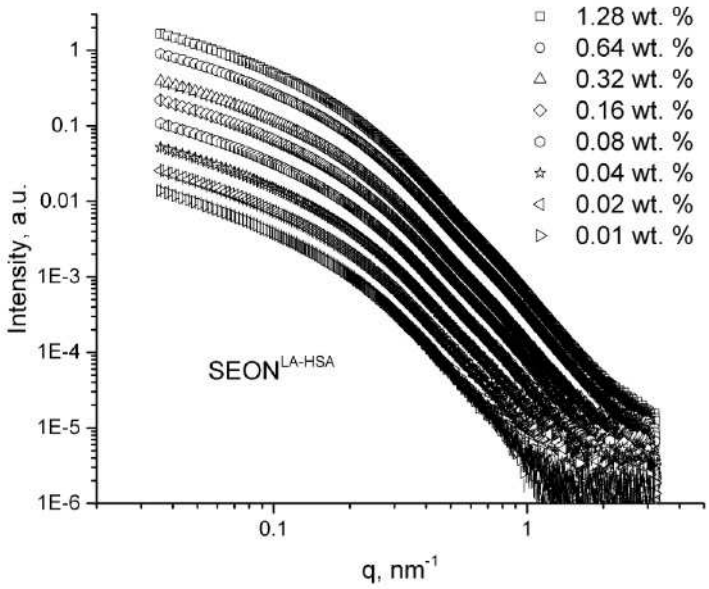

Figure S3. SAXS curves from the sample before the drug addition. The scattering intensity originating from the clusters of magnetic nanoparticle scales with concentration.

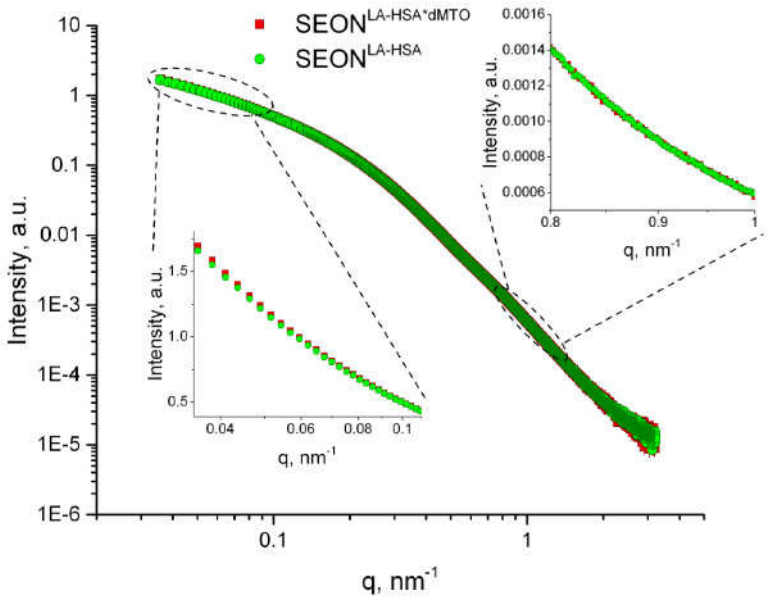

Figure S4. SAXS scattering curves from the samples with 1.28 wt. % of magnetic nanoparticles before and after the addition of dMTO. The curves were normalized to each other taking into account the points of the q-range 0.8-1.6 nm^{-1}. Error bars are smaller than the symbols. The two insets show the zoomed in intensities in two regions: high-q, where the intensities coincide, and low-q, where the intensity slopes differ due to the difference in the particle-particle interaction. This holds for the whole concentration series with the difference on the level of 2.5 – 3.5 % and well above the statistical uncertainty.

Indirect Fourier transformation

The indirect Fourier transformation (IFT) has been applied to the SAXS scattering curve from the SEON$^{LA\text{-}HSA}$ sample at the highest dilution (0.01 wt. %). Here we assume that the interparticle interaction is negligible and thus the cluster size can be probed. This is a model independent approach which is well suited for a qualitative analysis of the scattering data[32,41]

$$R_g^{\,2} = \frac{\int_0^{D_{\max}} p(r) r^2 dr}{2\int_0^{D_{\max}} p(r) dr},$$

where $D_{\max}$ is the upper limit for the particle dimension, and $p(r)$ is the pair distance distribution function of a particle. The $p(r)$ function is approximated by a linear combination of a finite number of cubic B-splines $\varphi_i(r)$

$$p(r) = \sum_{i=1}^{N} c_i \varphi_i(r),$$

where the expansion coefficients c_i are unknown parameters which can be determined from the scattering data using the IFT method. A large number ($N = 20-30$) of basic functions $\varphi_i(r)$ are used to describe $p(r)$ function, and there is no specific form or shape assumed in the IFT method. In the present study, the values of $D_{\max}$ were carefully chosen to give both good fittings of the experimental data and smooth $p(r)$ function. This selection procedure was performed by comparison of the results with different $D_{\max}$ values at intervals of 0.2 nm. From the indirect Fourier transformation the pair-distance distribution function was obtained (Figure S5). With the corresponding radius of gyration of 30.7 nm and the assumption of spherical nanoclusters their radius can be estimated to be around 39 nm.

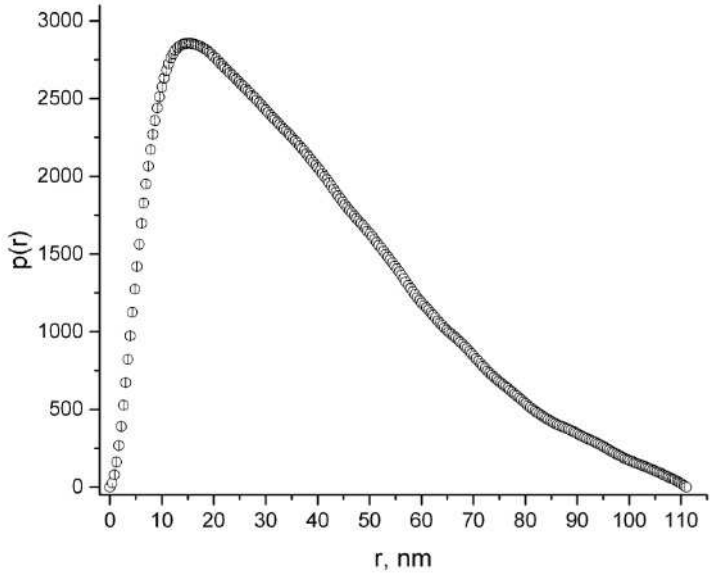

Figure S5. Pair distance distribution function as obtained from the indirect Fourier transformation of the SEON$^{LA\text{-}HSA}$ SAXS curve at 0.01 wt. %. Error bars are smaller than the symbols.

Structure of SEON$^{LA\text{-}HSA}$ *particles – freeze fracture TEM and FTIR*

Earlier studies revealed[11] that SEON$^{LA\text{-}HSA}$ consists of iron oxide nanoparticles of about 8.9 ± 2.2 nm in size, which are covered by a layer of albumin with a thickness of 1-3 nm. The hydrodynamic size of these multicore clusters is 70.8 ± 3.6 nm.

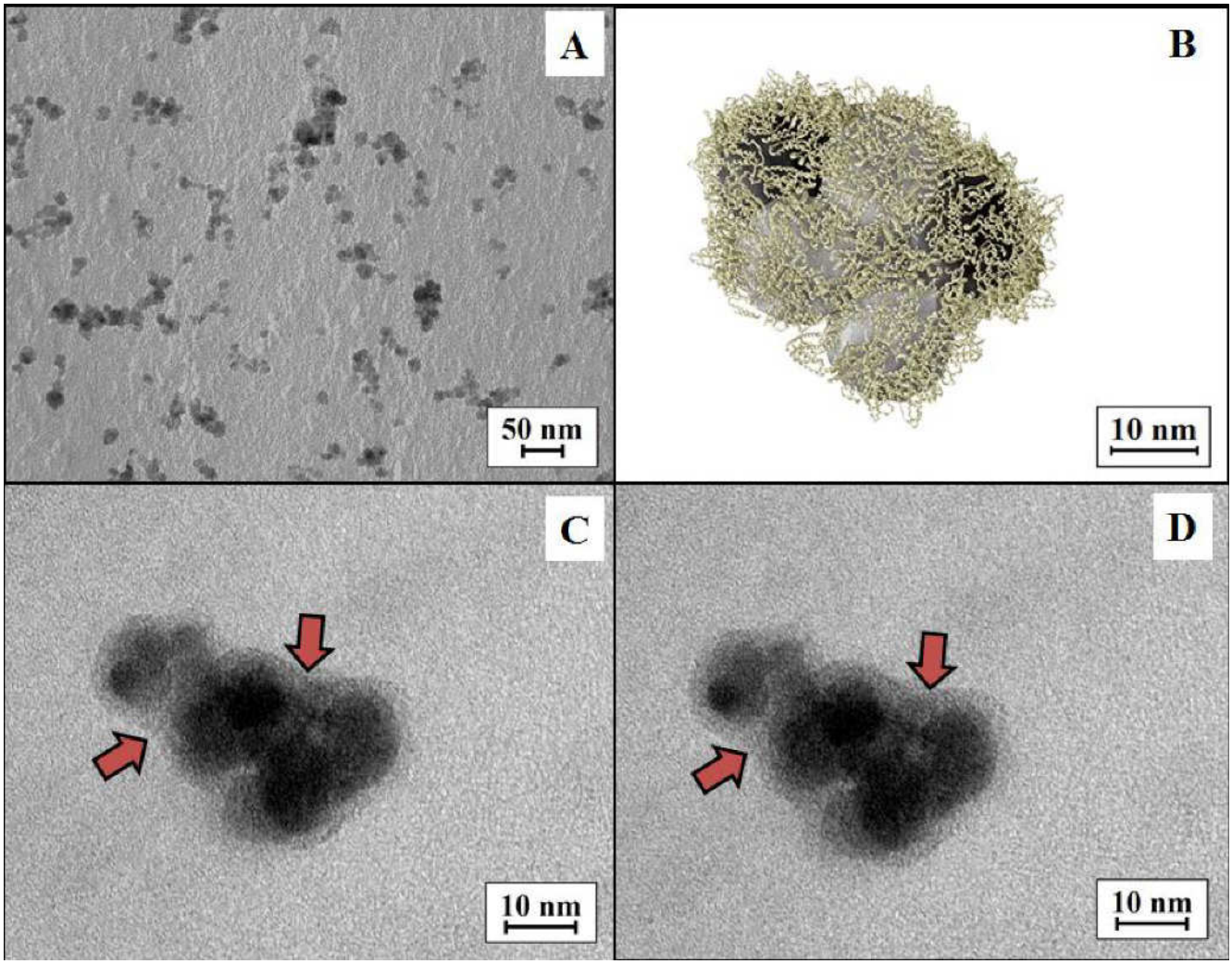

Figure S6. Freeze fracture-TEM images of SEON$^{LA\text{-}HSA}$. (**A**) Overview at a magnification of 25000. (**B**) in-scale model of iron oxide nanoparticles (d = 10 nm) and albumin (**C**) and (**D**) Detailed look on a single SEON$^{LA\text{-}HSA}$ cluster at a magnification of 150000 recorded from different focal planes. The arrows mark a clearly visible layer around the particle clusters. This image is taken from an earlier publication[11].

The FTIR spectra of SEON$^{LA\text{-}HSA}$, SEON$^{LA\text{-}HSA*MTO}$ and pure MTO are represented in Figure S7. The main peaks of SEON$^{LA\text{-}HSA}$ are clearly visible in both particle spectrums: the carboxylamide C-O stretching vibration at 1650 cm^{-1} and N-H deformation vibration at 1538 cm^{-1} and 1539 cm^{-1} derive from the protein, the Fe-O vibration at 626 cm^{-1} comes from the particles. The main peaks of MTO at

3466 cm^{-1} (O-H stretching) and 1612 cm^{-1} (aromatic C-O) cannot be detected in the $SEON^{LA\text{-}HSA*MTO}$ sample. This is due to the low (molar) amount of MTO functional groups compared to albumin.

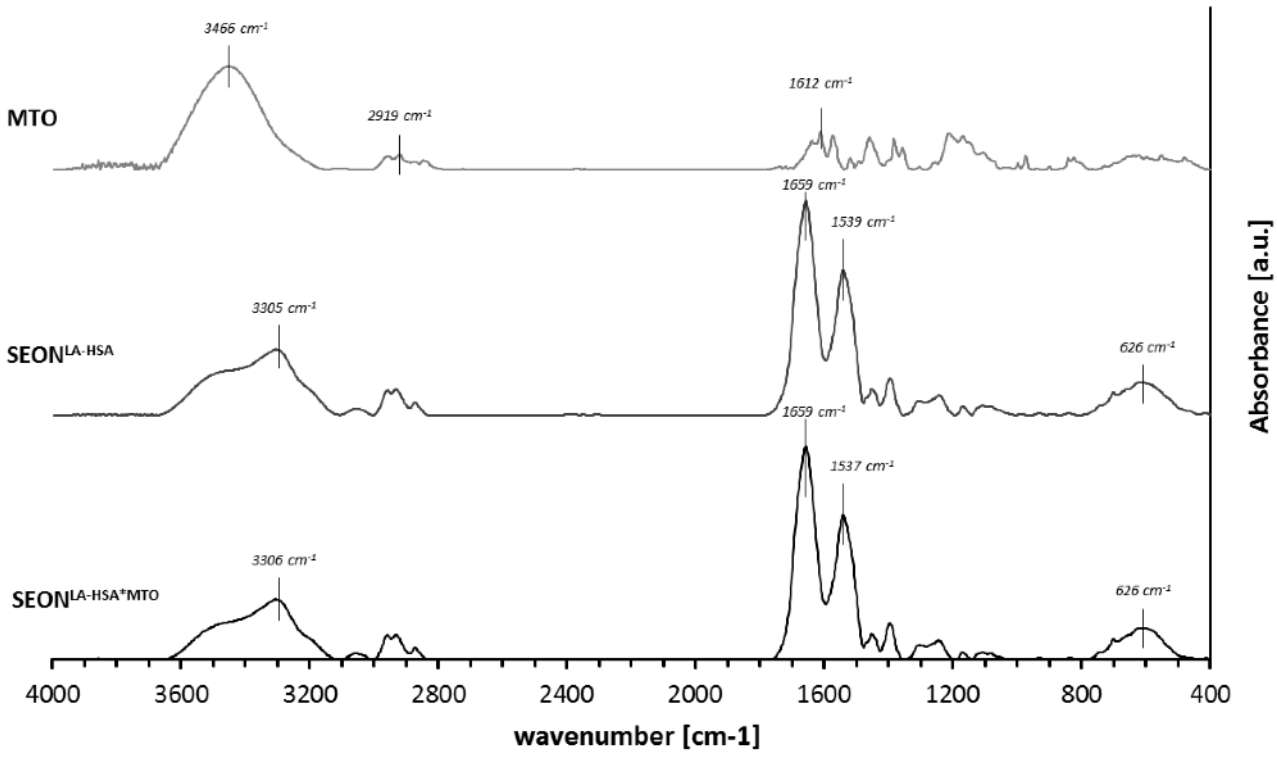

Figure S7. FTIR spectra of $SEON^{LA\text{-}HSA}$, $SEON^{LA\text{-}HSA*MTO}$ and pure MTO.

Results from Phosphate incubation assay

Results show that addition of up to 3.5 mM Phosphate (which equals more than two times the physiological phosphate concentration) does not enhance MTO release from $SEON^{LA\text{-}BSA}$ nanoparticles.

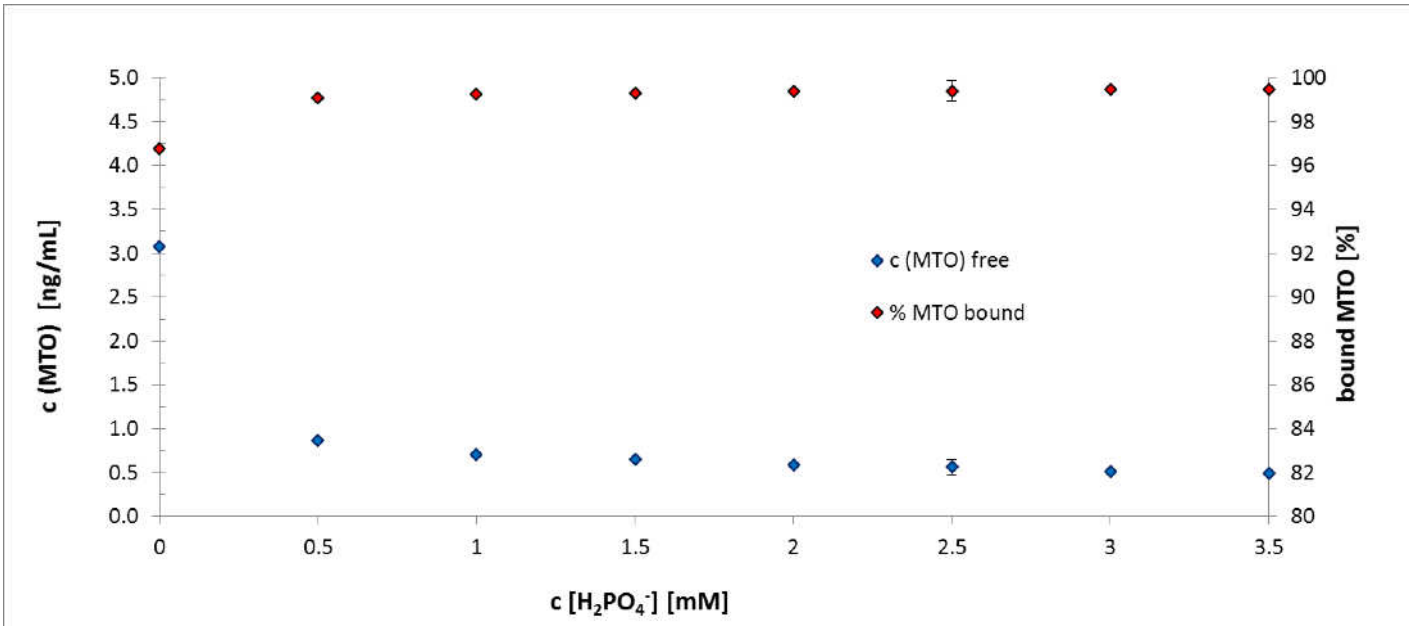

Figure S8. $H_2PO_4^-$ influence on MTO release from SEON nanoparticles. Absolute concentration of free MTO after incubation with phosphate is represented by the blue dots, relative percentage of particle-bound MTO is represented by the red dots.

Addition of different concentrations of phosphate did not lead to significant desorption of drug from the particle surface. In contrast, the binding rate of the drug (bound drug / total drug) even increased from 96.8 ± 0.06% to 99.5 ± 0.05% by addition of 3.5 mM phosphate.